Physical and Chemical Effects of CO2 and H2O Additives on Counterflow-Diffusion Flame Burning Methane

ARTICLE *in* ENERGY & FUELS · DECEMBER 2013

Impact Factor: 2.79 · DOI: 10.1021/ef401559r

5 AUTHORS, INCLUDING:

Lin Wang
Jilin University
349 PUBLICATIONS **2,939** CITATIONS

SEE PROFILE

Zhaohui Liu
Huazhong University of Science and Technology
94 PUBLICATIONS **618** CITATIONS

SEE PROFILE

energy&fuels

Article

pubs.acs.org/EF

Physical and Chemical Effects of CO_2 and H_2O Additives on Counterflow Diffusion Flame Burning Methane

Lin Wang,[†,‡] Zhaohui Liu,[*,†] Sheng Chen,[†] Chuguang Zheng,[†] and Jun Li[‡]

[†]State Key Laboratory of Coal Combustion, Huazhong University of Science and Technology (HUST), Wuhan, Hubei 430074, People's Republic of China

[‡]Thermal and Power Research Institute, Xi'an, Shaanxi 710032, People's Republic of China

ABSTRACT: A numerical study is conducted to understand better the flame structure in a $CH_4-O_2/N_2/CO_2/H_2O$ counterflow diffusion flame with various mole fractions of CO_2 and H_2O. Special interest is focused on the thermal, chemical, and diffusion effects of these species on the flame temperature and emission index of CO (EICO). A key result of the study is that the flame temperature is significantly reduced because of the chemical and thermal effects of CO_2. However, H_2O has a minor effect on the flame temperature, because its chemical effect almost cancels out its thermal effect. Meanwhile, the chemical effect of CO_2 induces the EICO to increase noticeably, although other effects of H_2O and CO_2 slightly decrease it. The diffusion effect of CO_2 only affects the distributions of the flame temperature and major species. Moreover, the pathways of fuel oxidation reactions are also investigated, and it is found that the low-temperature hydrocarbon reaction pathway (C_1 branch) becomes more active under oxy-fuel combustion conditions.

INTRODUCTION

Significant progress has been made recently in the research and demonstration of different technologies to meet the challenge of reduction of CO_2 emissions from combustion systems. Among those, one promising alternative is oxy-fuel combustion. For this combustion technology, instead of air in traditional combustion, pure oxygen is mixed with recycled flue gases as the oxidant. The flue gases are mainly composed of CO_2, H_2O, O_2, and a small mole fraction of N_2 because of air infiltration. The volume of emitted flue gas in the oxy-fuel combustion process is reduced by about 80%, as compared to conventional combustion in air.[1] It has been found that oxy-fuel combustion can reduce NO_x emissions to less than one-third of those in air combustion,[2−4] and attain slightly lower SO_2 emissions.[5]

To distinguish among the differences between the oxy-fuel and air combustions, some experimental studies have been conducted.[6−8] It has been found that the characteristics of the flame, such as temperature peak, ignition delay, etc., are greatly changed under oxy-fuel combustion conditions. After further research, these differences are found to be related to the chemical, thermal, and diffusive properties of CO_2 and H_2O in the oxidant.[2] Recently, the thermal effect of CO_2 has been numerically and experimentally studied for natural gas oxy-fuel combustion[9,10] with pure oxygen injection. However, in a practical oxy-fuel combustion system, the mole fraction of O_2 is lower than the mole fraction of CO_2. Under such conditions, only the chemical effect of CO_2 on the flame structure has been numerically and experimentally studied,[11−18] while the thermal and diffusion effects of CO_2 and H_2O are barely considered. Another critical issue for these numerical works is that the global or detailed chemical reaction mechanisms, i.e., GRI-Mech 3.0,[19] are usually used but have not been fully validated.

In the present work, the effects of the chemical, thermal, and diffusive properties of CO_2 and H_2O on the structure of a counterflow diffusion flame of methane were fully investigated, under typical oxy-fuel combustion conditions. To better analyze these effects, some artificial species were introduced and a well-validated detailed chemical reaction mechanism of oxy-fuel combustion, which involves 197 species and 779 elementary reactions,[20−23] was adopted. The flame temperature and emission index of CO (EICO) were analyzed to distinguish among the difference of these physical effects. Moreover, productions of intermediate radicals are integrated along with the distance. The great contributive radicals are chosen to illustrated the mitigation of reaction pathways under air and oxy-fuel combustion conditions.

NUMERICAL METHOD

An opposed jet diffusion flame, shown schematically in Figure 1, offers a convenient geometry for modeling the detailed combustion processes.

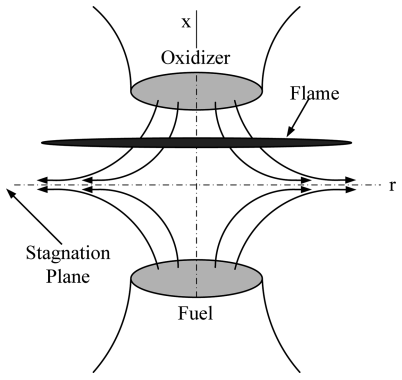

Figure 1. Schematic of the counterflow diffusion flame (x indicates the axial direction, and r indicats the radical direction).

Received: November 25, 2012
Revised: November 6, 2013
Published: November 6, 2013

The mathematical model adopted in this study is developed by Kee et al.[24] and extended by Lutz et al.[25] In the present $CH_4-O_2/N_2/CO_2/H_2O$ flame studied in this work, the temperatures and pressures of streams for both sides are 300 K and 1 atm, respectively. Moreover, the mole fraction of oxygen changes from 0.21 to 1.0. Meanwhile, the mole fraction of each species in the oxidizer side is defined as follows:

$$\alpha_i = X_i / \sum X_i \quad \text{where } i = O_2,\ CO_2,\ H_2O, \text{ and } N_2 \tag{1}$$

Here, X_i implies the volume fraction of a certain species. The mole fractions of CO_2 and N_2 vary correspondingly in the allowable range with a fixed value of O_2. The global strain rate a is obtained considering the balance of momentum flux[26,27]

$$a = \frac{-2V_O}{L}\left[1 + \frac{V_F}{-V_O}\sqrt{\frac{\rho_F}{\rho_O}}\right] \tag{2}$$

where L is the separation distance of two opposed jets; in the present study, $L = 2$ cm. V represents the velocity, and subscripts F and O mean the fuel and oxidizer, respectively. Moreover, the volume ratio between CH_4 and O_2 in fuel jet and oxidizer jets, respectively, is 1:2 for all cases.

The use of the mole fraction, which includes the information of convection and diffusion source terms, is not appropriate to grasp the behavior of CO. Nishioka et al.[28] suggested the following EICO:

$$\mathrm{EICO} = \frac{\int_0^L W_{CO}\dot{w}_{CO}\mathrm{d}x}{-\int_0^L W_{CH_4}\dot{w}_{CH_4}\mathrm{d}x} \tag{3}$$

where W_i and $\dot{w}_i$ are the molecular weights and molar production rates of ith species, respectively.

A program for computing opposed-flow diffusion flames, OPPDIF,[25,29,30] is chosen to solve the governing equations. The flame radiation is calculated by adding a radiation source term to the energy equation of OPPDIF

$$\rho u\frac{\mathrm{d}T}{\mathrm{d}x} - \frac{1}{c_p}\frac{\mathrm{d}}{\mathrm{d}x}\left(\lambda\frac{\mathrm{d}T}{\mathrm{d}x}\right) + \frac{\rho}{c_p}\sum_i c_{pi}Y_iV_i\frac{\mathrm{d}T}{\mathrm{d}x} + \frac{1}{c_p}\sum_i h_i\dot{\omega}_i - \dot{q} = 0 \tag{4}$$

where ρ is the mass density, u is the axial velocity, and c_p is the heat capacity at constant pressure. Y_i, V_i, and h_i are the mass fractions, diffusion velocities, and enthalpies of ith species, respectively. $\dot{q}$ is the flame radiation heat flux and is calculated using an optically thin radiation model with the Planck mean absorption coefficient.

$$\dot{q} = -4\sigma K_p(T^4 - T_a^4) \tag{5}$$

$$K_p = \sum_{i=1}^{4} P_iK_i \quad \text{where } i = CO_2,\ H_2O,\ CH_4, \text{ and } CO \tag{6}$$

where $\sigma = 5.669 \times 10^8\ \mathrm{W\ m^{-2}\ K^{-4}}$ is the Stefan–Boltzmann constant, K_i is the Planck mean absorption coefficient,[31−35] and P_i is local partial pressure of the specific species. T and T_a are the local and ambient temperatures, respectively.

In Figure 2, it shows the variation of the heat capacity of N_2, CO_2, and H_2O under different temperatures according to the thermal database.[19] Generally, the specific heat capacity (C_p) of CO_2 is much higher than that of N_2, which may induce distinct flame characteristics under oxy-fuel combustion conditions.

To aid the analysis, artificial species X, X', Y, and Y' were introduced. X and Y have the same thermal and transport properties of CO_2 and H_2O, respectively, but they are not allowed to participate in any chemical reaction. Therefore, X and Y are strictly regarded as chemically inert species. Artificial species X' and Y' have the same transport properties as those of CO_2 and H_2O, respectively, while their thermal properties remain the same as N_2, and they do not participate in any chemical reaction. Therefore, X' and Y' are strictly regarded as thermal and chemical inert species.

Moreover, observable diffusion coefficients of CO_2 and N_2 versus different temperatures under different conditions according to Mostinsky et al.[36] are shown in Figure 3 to help to analyze the diffusion effect of CO_2 on the flame. To identify its effect, another artificial species CO_2* is introduced, which has the same thermochemical property as CO_2, but the diffusion property is the same as N_2. The difference between the additive cases of CO_2 and CO_2* is, thus, due to the diffusion effect.

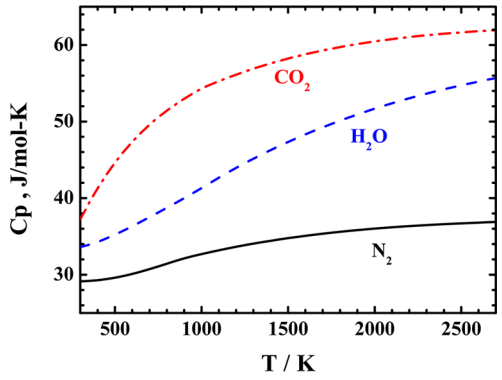

Figure 2. Specific heat capacity of N_2, CO_2, and H_2O under different temperatures.

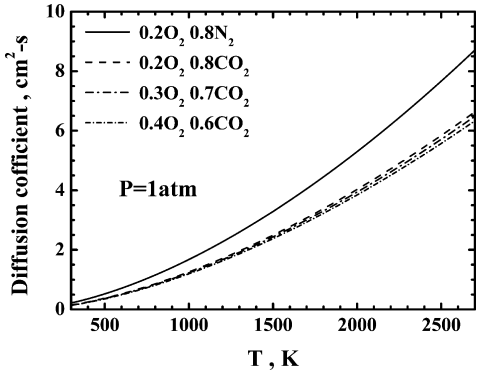

Figure 3. Observable diffusion coefficient of CO_2 and N_2 through binary gas mixtures under $p = 1$ atm.

RESULTS AND DISCUSSION

Thermal and Chemical Effects of CO_2. Figure 4 shows the variation of the maximum flame temperature at various mole fractions of O_2 in the oxidizer stream, with CO_2, X, and X' as additives. The differences of predictions for the flame temperature

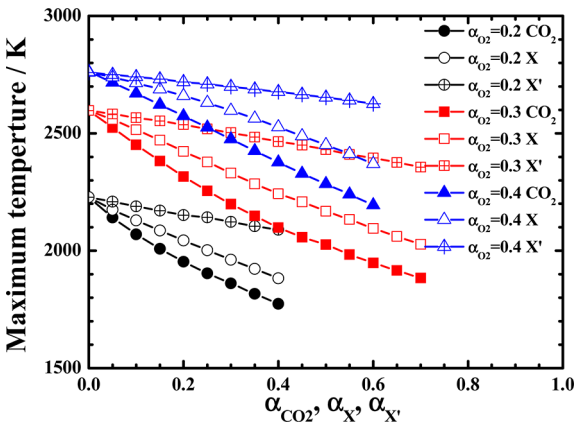

Figure 4. Variation of the maximum flame temperature with the mole fraction of CO_2, X, and X' for various mole fractions of O_2 in the oxidizer stream at the strain rate of 100 $\mathrm{s^{-1}}$.

dx.doi.org/10.1021/ef401559r | Energy Fuels 2013, 27, 7602−7611

between X' and X additive cases are due to the thermal effect. Besides, the difference between the additive cases of CO_2 and the artificial species X is, thus, due to the chemical effect.

The results show that both the thermal and chemical effects of CO_2 make the flame temperature decrease. It is easily understood that the result of the thermal effect is mainly due to the higher heat capacity of CO_2. Meanwhile, the main factor for the chemical effect is the thermal dissociation of CO_2.[11] It can be explained from two aspects. One aspect is that the process of the thermal dissociation of CO_2 is endothermic, which is quite noticeable at high mole fractions of CO_2 under oxy-fuel conditions. The other aspect is that the thermal dissociation of CO_2 breaks the chemical equilibrium for some reactions that are relative to the production of CO. This makes the production and oxidation of CO take a longer time. Therefore, the heat release is slow.

Moreover, the thermal and chemical effects of CO_2 on the EICO are displayed in Figure 5. The result shows that the

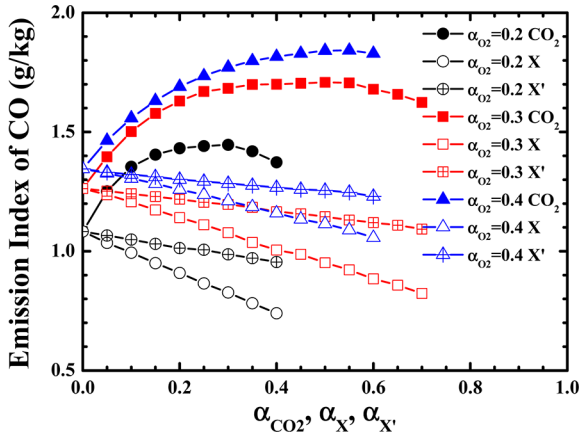

Figure 5. Variation of EICO with the mole fraction of CO_2, X, and X' for various mole fractions of O_2 in the oxidizer stream at the strain rate of 100 s^{-1}.

thermal property of CO_2 affects the production of CO in the whole chemical reaction space and reduces the EICO. However, when considering the chemical effect of CO_2, things change. The chemical effect of CO_2 greatly increases the EICO. It can be observed that the degree of ECIO growth becomes larger as the mole fraction of CO_2 increases. Obviously, the chemical effect of CO_2 on the EICO is greater than the thermal effect of CO_2. Another interesting thing is that, when the mole fraction of CO_2 exceeds a certain value, the EICO decreases slowly. Hereafter, it is called the saturation effect of CO_2.

To further identify how the thermal and chemical properties of CO_2 affect the reaction pathways, the production rate of CO for all elementary reactions has been selected and analyzed. Panels a and b of Figure 6 show the contribution of thermal and chemical properties, respectively.

As shown in Figure 6a, there are two elementary reactions that mainly contribute to the production rate of CO in the selected condition (30% O_2 and 70% X and X').

$$CO + OH = CO_2 + H \quad \text{(R34)}$$

$$HCO = H + CO \quad \text{(R49)}$$

R49 shows a positive effect on the production rate of CO, but R34 shows a negative effect on it. When X replaces X', the production rate of CO for R49 increases slightly; meanwhile, the adverse effect of R34 on the production rate of CO is enlarged

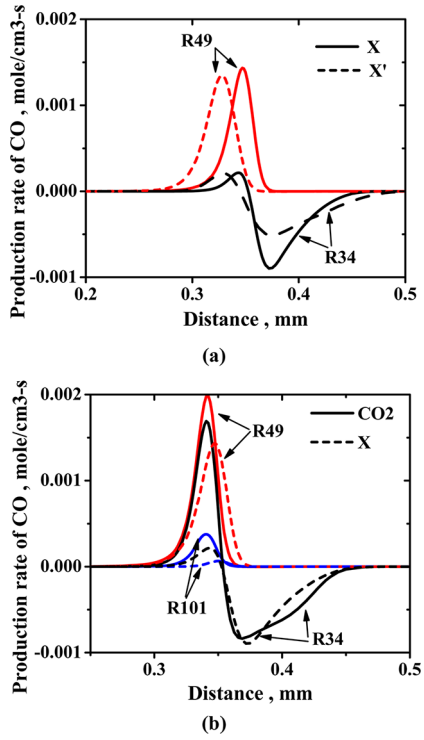

Figure 6. (a) Production rate of CO for different elementary reactions with 70 vol % X and X' and 30 vol % O_2 at the strain rate of 100 s^{-1}. (b) Production rate of CO for different elementary reactions with 70 vol % CO_2 and X and 30 vol % O_2 at the strain rate of 100 s^{-1}.

greatly. Obviously, the enlarged adverse effect of R34 by the thermal effect of CO_2 helps to reduce the EICO.

For comparison, the difference in the production rate of CO between the cases using CO_2 and X is also shown in Figure 6b under the corresponding conditions. It illustrates that, in addition to R34 and R49, another reaction also shows great effect on the production of CO.

$$CH_2(s) + CO_2 = CH_2O + CO \quad \text{(R101)}$$

Moreover, the effect of both R49 and R101 is positive. R34 has both positive and negative effects in the whole combustion space. Among those, the positive effects of all of these elementary reactions are greatly enhanced when X is replaced by CO_2. Meanwhile, the adverse effect of R34 does not change so much. Owing to the thermal dissociation of CO_2,[11] the production of CO in R34 and R101 greatly increases. According to the chemical equilibrium, the production of H greatly decreases and then further makes the production of CO in R49 greatly increased.

Also, to better understand the saturation effect of CO_2, the production rate of CO for all elementary reactions under 30% O_2 and various mole fractions of CO_2 conditions has been analyzed in detail. It is found that, for some reactions, the trend of transformation for the production rate of CO highly coincides with the variation of EICO, which is described above. As shown in Figure 7, besides R34 and R49, another two important elementary reactions are

$$C_2H_2 + O = CH_2 + CO \quad \text{(R237)}$$

$$CH_2CO + H = CH_3 + CO \quad \text{(R317)}$$

It is explained that, as the mole fraction of CO_2 increases, the chemical equilibrium makes it advantageous for the increasing production of CO. However, productions of H, O, and HCO

dx.doi.org/10.1021/ef401559r | Energy Fuels 2013, 27, 7602−7611

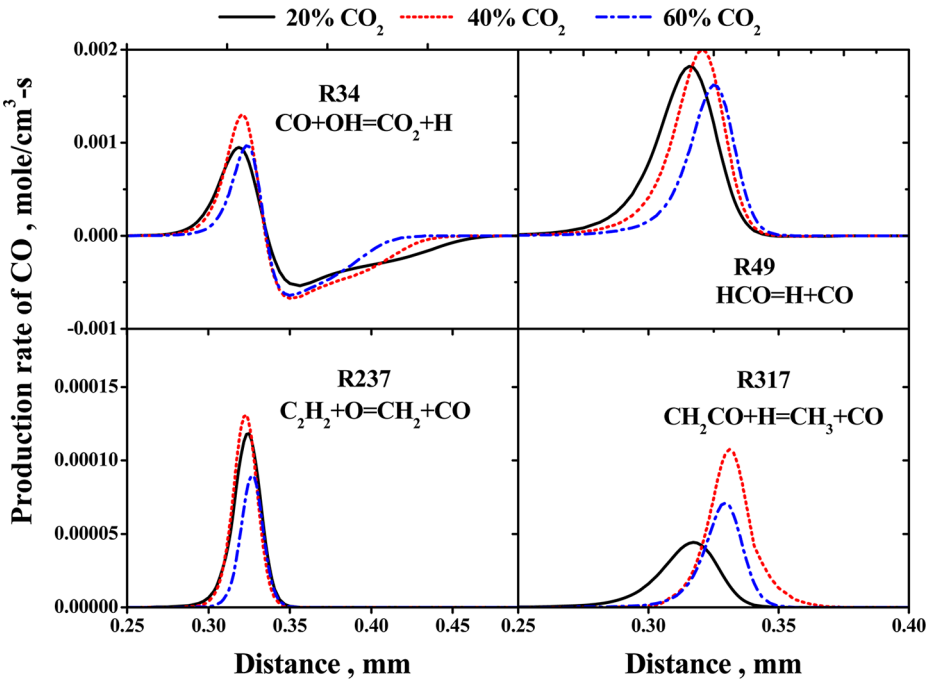

Figure 7. Production rates of CO for some elementary reactions for various mole fractions of CO_2 under a 30% O_2 condition.

decrease when the mole fraction of CO_2 exceeds about 40%. This is due to the inhibition effect of the thermal dissociation of CO_2.[3] Therefore, for a higher mole fraction of the CO_2 condition, the chemical equilibrium just restrains the production rate of CO, instead of making it further increase.

Thermal and Chemical Effects of H_2O. For oxy-fuel combustion, besides CO_2, H_2O is usually included in the oxidant stream. In wet recirculation combustion (the flue gas is partially recirculated without drying), the mole fraction of H_2O in the oxidant stream may be as high as 30 vol %. Therefore, it is essential to understand the effect of H_2O on the flame under oxy-fuel combustion conditions.

Artificial species *Y* and *Y′* are introduced to clearly identify the thermal effects of H_2O in the oxidant stream, and the results are shown in Figure 8. Thermal effects of H_2O can also decrease the flame temperature because of its higher heat capacity. Meanwhile, the difference between the additive cases of H_2O and the artificial species *Y* is due to chemical effects. The result in Figure 8 shows that the chemical effect of H_2O slightly increases the flame temperature. The degree of temperature growth/reduction becomes larger with the increase in the concentration of the artificial species.

Also, the thermal and chemical effects of H_2O on EICO are displayed in Figure 9. It is clear that both the thermal and chemical effects of H_2O help to reduce the EICO. The degree of EICO reduction also becomes larger with the increase in the concentration of artificial species.

To understand how H_2O affects the chemical oxidation, Figure 10 displays the variations of production rates of CO, H, and OH with their important related elementary reactions. The condition is fixed at 30% O_2/60% CO_2 and a strain rate of 100 s^{-1}. The most important elementary reactions for CO are R34, R49, and R101. It is obvious that, when H_2O is added to the oxidant stream, the production rates of CO decrease. It is anticipated that the dissociation of H_2O greatly affects the distributions and productions of H and OH radicals, which are important for the production of CO. As concluded, important

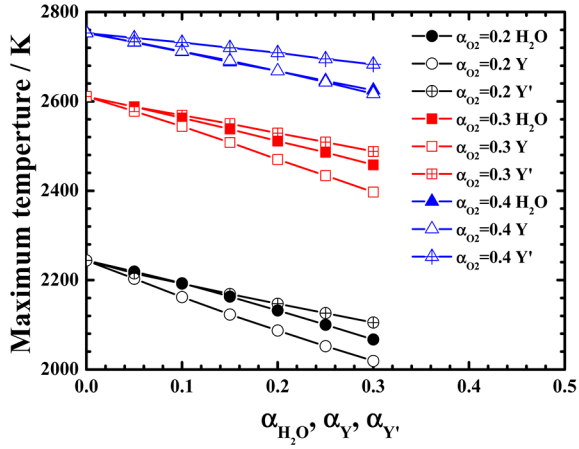

Figure 8. Variation of the maximum flame temperature with the mole fraction of H_2O, *Y*, and *Y′* for various mole fractions of O_2 in the oxidizer stream at the strain rate of 100 s^{-1}.

elementary reactions for the production of H are shown in Figure 10; they are

$$O + H_2 = OH + H \quad (R12)$$

$$OH + H + M = H_2O + M \quad (R14)$$

$$OH + H_2 = H + H_2O \quad (R15)$$

Besides R12, R14, and R15, another two elementary reactions are important for the production of OH.

$$OH + OH = O + H_2O \quad (R13)$$

$$CH_2O + OH = HCO + H_2O \quad (R46)$$

When H_2O is added in the oxidant stream, the production rates of H in R12, R14, and R15 decrease. In particular, R15 contributes mostly to reduce the production of H. However, R13 and R15 mainly increase the production of OH. In R46, according to the chemical equilibrium, it is also easily understood that the

dx.doi.org/10.1021/ef401559r | *Energy Fuels* 2013, 27, 7602−7611

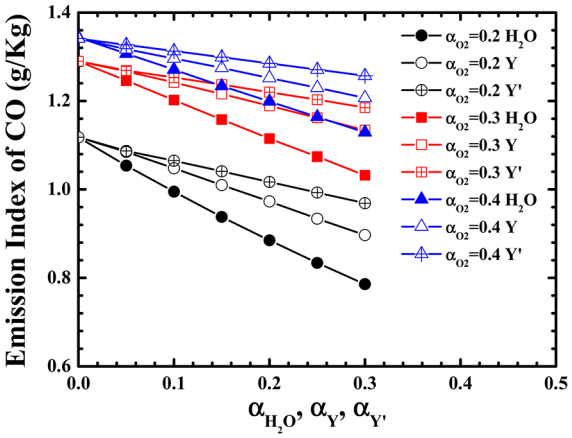

Figure 9. Variation of EICO with the mole fraction of recirculated H_2O, Y, and Y' for various mole fractions of O_2 in the oxidizer stream at the strain rate of 100 s^{-1}.

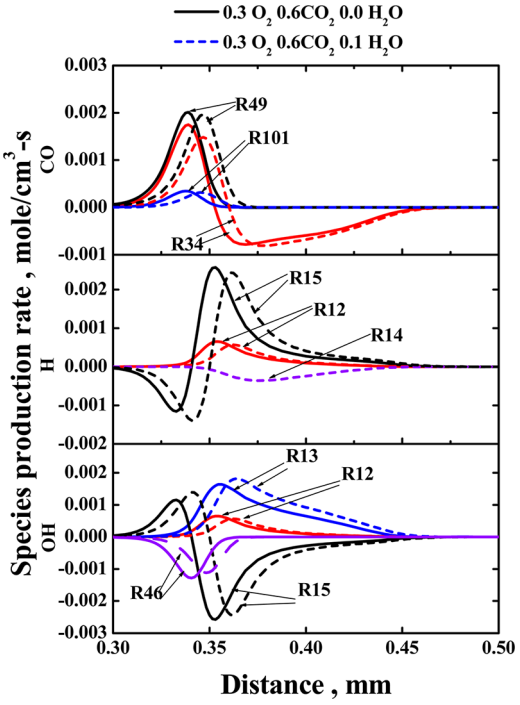

Figure 10. Production rate of some key species for different elementary reactions under 30 vol % O_2 and 60 vol % CO_2 with and without H_2O at the strain rate of 100 s^{-1}.

production rate of HCO decreases and the production rate of CH_2O increases when H_2O is added.

Therefore, because of the decrease of H and the increase of OH, the production rate of CO decreases for R34 after H_2O addition. Moreover, the decrease of HCO/increase of CH_2O induces the production rates of CO in R49 and R101 to decrease, respectively.

Effect of the Mass Diffusion of CO_2. Major species and temperature distributions are illustrated in Figure 11a under 21% O_2 and 79% CO_2 conditions at the strain rate of 100 s^{-1}. It shows that distributions of major species and flame temperature change, when considering the change in diffusion properties. The position of the maximum temperature moves closer to the fuel side for the CO_2 additive case. From Figure 3, it is clear that the observable diffusion coefficient of N_2 is larger than that of CO_2.

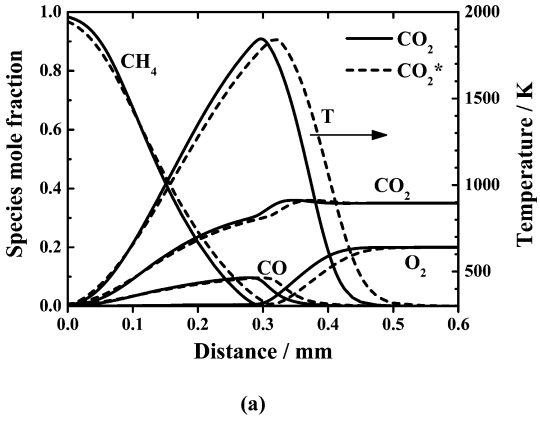

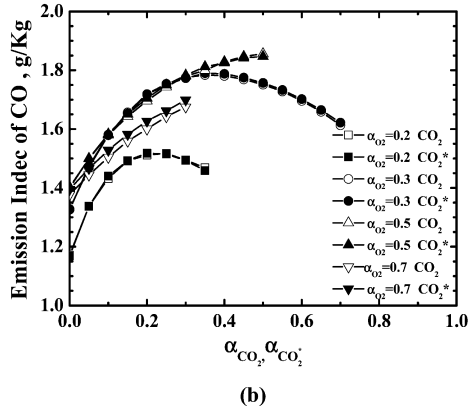

Figure 11. (a) Major species distribution under 21% O_2 and recirculated 79% CO_2 and CO_2* at the strain rate of 100 s^{-1}. (b) Variation of EICO with the mole fraction of recirculated CO_2 and CO_2* for various oxygen mole fractions in the oxidant stream at the strain rate of 100 s^{-1}.

In other words, oxygen in CO_2* (diffusion property is the same as N_2) diffuses faster than that in CO_2. Thus, for the CO_2 additive case, O_2 is consumed later and the higher temperature zone is closer to the oxidizer side. Moreover, Figure 11b displays the prediction of EICO under various mole fractions of CO_2 and CO_2* at the strain rate of 100 s^{-1}. It can be noted that the diffusion of CO_2 only affects the distribution of the temperature and the major species, with a negligible effect on the maximum flame temperature and the emissions of CO.

Overall Effect of CO_2 and H_2O. Actually, for retrofitting of the current air combustion boiler with the oxy-fuel combustion technology, the heat transfer by the oxy-fuel combustion condition should be similar to that of the air combustion condition to minimize changes. Usually, part of the flue gas is recirculated and mixed with the pure oxygen to be the oxidant for oxy-fuel combustion. Dependent upon whether water is removed from the flue gas that is recirculated, the recirculation is called dry or wet recirculation. In the present work, the configuration for oxy-fuel combustion with dry recirculation (OCDR) is 25% O_2, 70% CO_2, and 5% H_2O, while the configuration for oxy-fuel combustion with wet recirculation (OCWR) is 30% O_2, 50% CO_2, and 20% H_2O.

To understand better the overall effect of CO_2 and H_2O on the flame temperature and EICO, under OCDR or OCWR, several numerical simulations have been conducted at the strain rate of 100 s^{-1}. The volumetric fractions of species for the oxidizer jet have been displayed in Table 1. There, Sim2−Sim6 cases have been compared to each other to clarify the overall effect of CO_2, under OCDR conditions. Among those, Sim6 can be regarded as a base case. Sim7−Sim11 cases have been compared to clarify the

dx.doi.org/10.1021/ef401559r | Energy Fuels 2013, 27, 7602−7611

Table 1. Volumetric Fraction of Species of Oxidizer Jet for Several Cases under OCDR and OCWR at Φ = 1.0

	O_2 (%)	CO_2 (%)	H_2O (%)	X (%)	X' (%)	Y (%)	Y' (%)
Sim1	20				80		
Sim2	25				70		5
Sim3	25			70			5
Sim4	25	70					5
Sim5	25	70				5	
Sim6	25	70	5				
Sim7	30				50		20
Sim8	30			50			20
Sim9	30	50					20
Sim10	30	50				20	
Sim11	30	50	20				

overall effects of CO_2 and H_2O, under OCWR conditions. Among those, Sim11 can be regarded as a base case.

The overall effects of CO_2 and H_2O on the temperature, under OCDR and OCWR, have been illustrated in Figure 12a. For either OCDR or OCWR, both the thermal and chemical effects of CO_2 induce the flame temperature decrease and the thermal effect shows the greatest importance. However, for OCWR, the proportion of the chemical effect of CO_2 on the flame temperature increases. Moreover, thermal and chemical effects of H_2O on the flame temperature almost cancel each other out; therefore, the existence of H_2O hardly affects the flame temperature. The overall effect of CO_2 makes the flame temperature greatly decrease from 2180 to 1765 K under OCDR and from 2359 to 1966 K under OCWR.

The overall effects of CO_2 and H_2O on the EICO, under OCDR and OCWR, have been illustrated in Figure 12b. Except for the chemical effect of CO_2, other properties of CO_2 and H_2O make the EICO decrease for both OCDR and OCWR. However, the chemical effect of CO_2 shows the greatest importance. Moreover, the contributive proportion of the chemical effect of CO_2 in the overall effects increases under OCWR increases. For OCDR, the overall effects of CO_2 and H_2O are to increase the EICO by 0.358 g/kg. For OCWR, the overall effects of CO_2 and H_2O are to increase the EICO by 0.340 g/kg. Therefore, it can be concluded the overall effect of CO_2 and H_2O is increasing EICO, under both OCDR and OCWR conditions.

Because of significant changes in the reactive atmosphere, the chemical oxidation pathway for hydrocarbon fuel under oxy-fuel combustion conditions is largely different from that under air combustion conditions. Contributed values for the intermediate radicals are calculated on the basis of the integration of the production rates for each elementary reaction in the whole reaction distance[37]

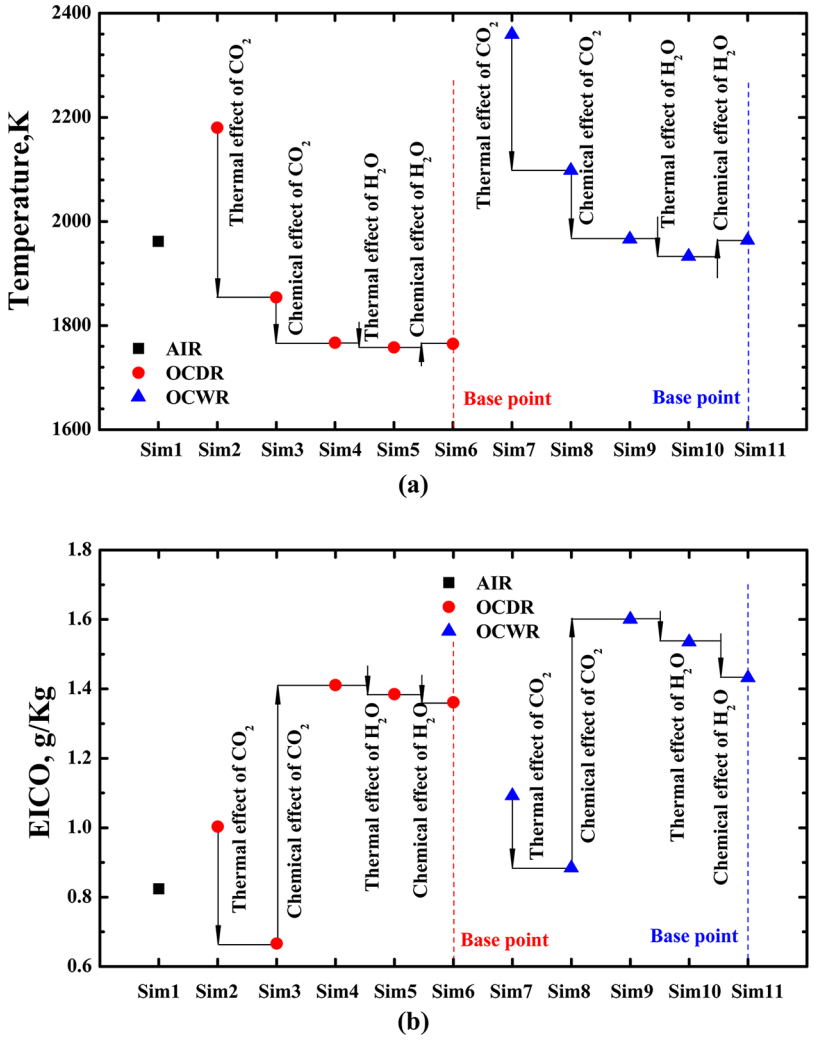

Figure 12. Overall effect for both CO_2 and H_2O on the (a) temperature and (b) EICO under OCDR and OCWR conditions at the strain rate of 100 s^{-1}.

dx.doi.org/10.1021/ef401559r | *Energy Fuels* 2013, 27, 7602−7611

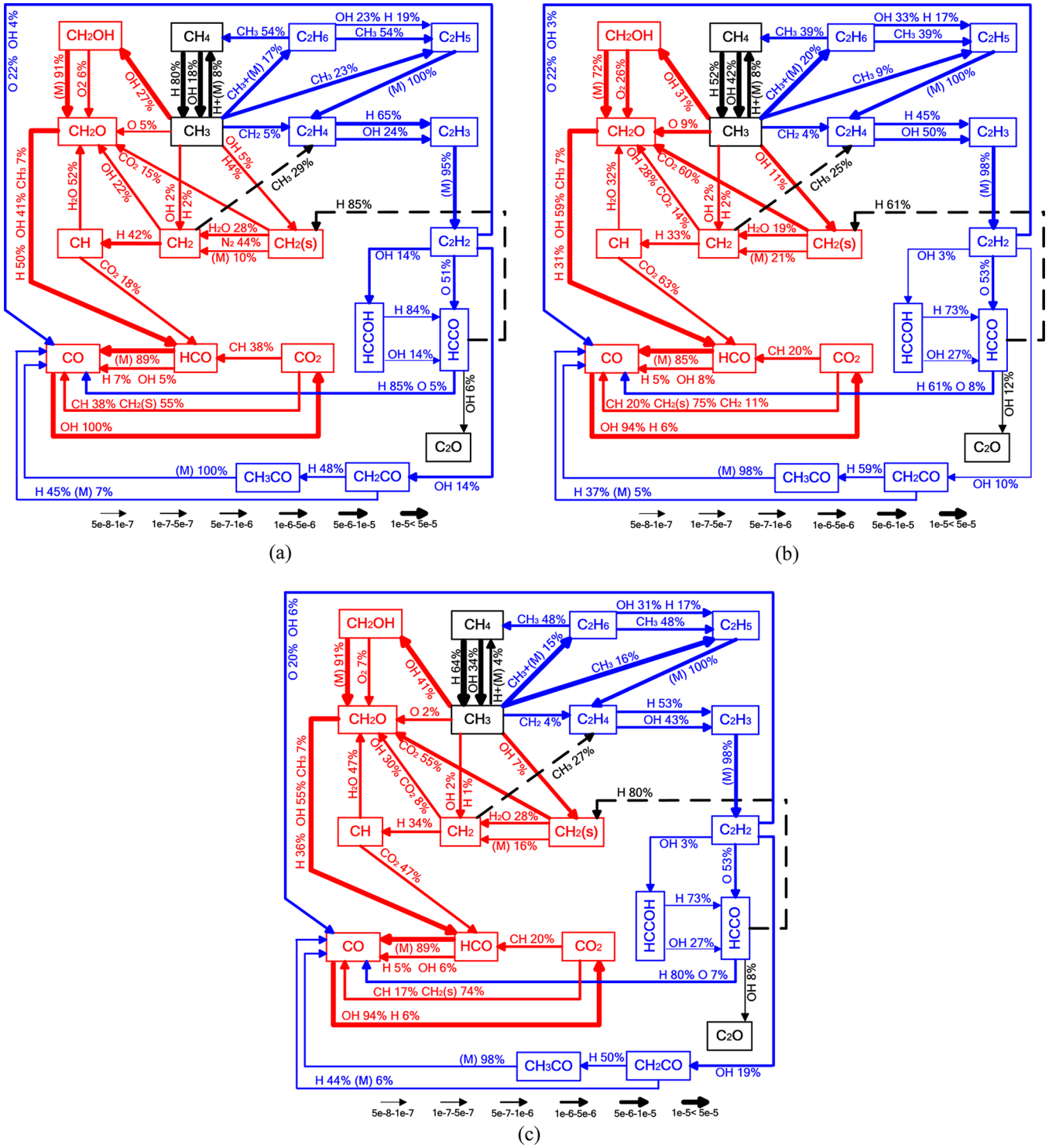

Figure 13. Fuel oxidation reaction pathways for (a) AC, (b) OCDR, and (c) OCWR at the strain rate of 100 s^{-1}.

$$A_i = \int_L^0 \dot{w}_i \mathrm{d}x \tag{17}$$

where $\dot{w}_i$ is the mole production rate of ith species and A_i is the mole flow rate of ith species in the present work. Here, we consider the consumption of species and the mole contribution ratio C_i of ith species is defined as follows:

$$C_i = |A_i| / \sum |A_i| \quad \text{where } A_i < 0 \tag{18}$$

On the basis of the mole contribution ratio, oxidation reaction pathways for CH_4 under air combustion (AC), OCDR, and OCWR at the strain rate of 100 s^{-1} are shown in Figure 13. For the three combustion conditions, a H atom is initially extracted from CH_4 to form CH_3. Then, this radical is oxidized by two typical pathways: the C_1 and C_2 branch pathways. C_1 branch pathways are mainly composed of two lines: $CH_3 \rightarrow [CH_2OH, CH_2, CH_2(s), \text{and } CH] \rightarrow CH_2O \rightarrow HCO \rightarrow CO \rightarrow CO_2$ and $CH_3 \rightarrow [CH_2 \text{ and } CH_2(s)] \rightarrow CH \rightarrow HCO \rightarrow CO \rightarrow CO_2$. The two lines correspond to a low-temperature oxidation process.

dx.doi.org/10.1021/ef401559r | *Energy Fuels* 2013, 27, 7602−7611

C_2 branch pathways, which correspond to a high-temperature oxidation process, contain a typical line: $CH_3 \rightarrow C_2H_6 \rightarrow C_2H_5 \rightarrow C_2H_4 \rightarrow C_2H_3 \rightarrow C_2H_2 \rightarrow CO \rightarrow CO_2$. There, C_2H_2 is oxidized to CO directly or through further conversion of HCCO and CH_2CO. Moreover, C_1 and C_2 branch pathways interact through the paths of $CH_2 \rightarrow C_2H_4$ and $HCCO \rightarrow CH_2(s)$.

To identify the difference between the C_1 and C_2 branch pathways, the ratio between the summations of the mass flow contribution ratio for the two branches is calculated and called the C_1-C_2 ratio. C_1-C_2 ratios are 1.23, 1.88, and 2.04 under AC, OCDR, and OCWR, respectively. This means that C_1 branch pathways become more dominant under oxy-fuel combustion conditions compared to those in air combustion conditions.

Moreover, the mole contribution ratios for some important intermediate reaction paths under different combustion conditions are compared and displayed in Table 2. As calculated,

Table 2. Comparisons of the Mass Flow Contribution Ratios for Some Important Intermediate Reaction Paths under Different Combustion Conditions

	radical species	AC (%)	OCDR (%)	OCWR (%)
$CH_4 \rightarrow CH_3$	H	80	52	64
	OH	18	42	34
$CH_3 \rightarrow CH_2OH$	OH	27	31	41
$CH_3 \rightarrow CH_2(s)$	H	4		
	OH	5	11	7
$CH_2OH \rightarrow CH_2O$	M	91	72	91
	O_2	6	26	7
$CH_2O \rightarrow HCO$	H	50	31	36
	OH	41	59	55
$CH_2(s) \rightarrow CH_2O$	CO_2	15	60	55
$CH \rightarrow HCO$	CO_2	18	63	47
$CH_3 \rightarrow C_2H_5$	CH_3	23	9	16
$HCCO \rightarrow CH_2(s)$	H	85	61	80
$C_2H_6 \rightarrow C_2H_5$	OH	23	33	31
	CH_3	54	39	48
$C_2H_4 \rightarrow C_2H_3$	OH	24	45	53
	H	65	50	43
$CO \rightarrow CO_2$	OH	100	94	94
	O		6	6

the mole contribution ratio of OH increases and that of H decreases for the path of $CH_4 \rightarrow CH_3$ and its two branches, when the combustion conditions change from air to oxy-fuel combustion. Another noticeable difference under oxy-fuel combustion conditions is that the mole contribution ratio of CO_2 in some C_1 branch paths, such as $CH_2(s) \rightarrow CH_2O$ and $CH \rightarrow HCO$, is enhanced greatly. That also suggests that the production rates of CO are apparently different from the AC conditions.

Furthermore, the oxidation rate of each elementary reaction is integrated in the entire reaction distance for the opposed diffusion flame under AC, OCDR, and OCWR conditions. It is found that there are 29 elementary reactions that have notable changes for their integrated oxidation rates, and they are illustrated in Figure 14. These elementary reactions are displayed in the Appendix in detail.

From AC to OCDR, there are reaction rates (R34, R43, R46, R49, R60, R122, R124, etc.) in which the integrated oxidation rate increases. Also, the importance of R30 and R91 is highlighted. These reactions mainly exist in the C_1 branch pathways and help to enhance the production of CO. R81, R93, R107, R199, R201, and R330 help to reduce the production rates of CO. Moreover, when it changes from OCDR to OCWR, R67, R70, R101, etc. help to reduce the production of CO, even though the modification is not very noticeable compared to the changes between AC and OCDR. It still helps to reduce the emissions of CO.

CONCLUSION

A numerical study on the flame structure of $CH_4-O_2/N_2/CO_2/H_2O$ counterflow diffusion flames was conducted at the strain rate of 100 s^{-1}. Various mole fractions of CO_2 and H_2O were tested to investigate the thermal, chemical, and diffusion effects of CO_2 and H_2O on the flame. The following conclusions can be summarized: (1) Both the thermal and chemical effects of CO_2 help to reduce the flame temperature. However, the thermal and chemical effects of H_2O on the flame temperature almost cancel each other out. The chemical effect of CO_2 induces the EICO increase noticeably, although other effects of H_2O and CO_2 nearly cancel it out. Simultaneously, diffusion property of CO_2 minimally affects the flame temperature and the EICO but significantly affects their distributions. (2) In oxy-fuel combustion conditions, R34, R49, and R101 mostly contribute to the production rate of CO when considering both the thermal and chemical effects of CO_2. When H_2O is added, the production rate of H decreases and that of OH increases, which makes the production rate of CO decrease further. Because of the effect of R34, R49, R237, and R317, the emission of CO initially increases but then decreases with the increase of CO_2. (3) There are two C_1 branch pathways and one C_2 branch pathway that mainly contribute to the oxidation of CH_4. When combustion changes from air to oxy-fuel, the mole contribution ratio of OH in the reaction pathways increases, while that of H decreases. Meanwhile, CO_2 greatly activates the oxidation of CH and $CH_2(s)$.

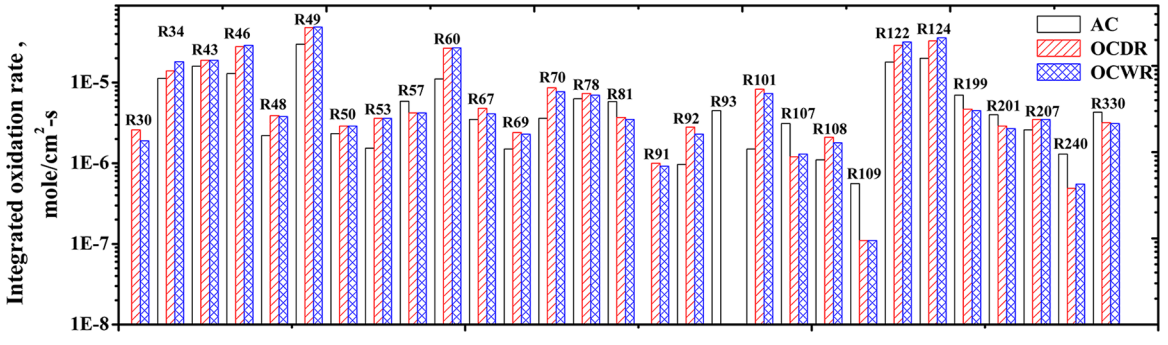

Figure 14. Elementary reactions in which the oxidation rates change greatly for AC, OCDR, and OCWR at the strain rate of 100 s^{-1}.

dx.doi.org/10.1021/ef401559r | Energy Fuels 2013, 27, 7602−7611

Table A1. Elementary Reactions with Great Changes for Their Integrated Oxidation Rates under Different Combustion Conditions

	A (m, mol, and s)	B	E_a (J/mol)
$CO + O + (M) = CO_2 + (M^a)$ (R30)	1.80×10^4	0	9.97×10^6
low-pressure limit	1.40×10^{24}	−2.79	1.75×10^7
$CO + OH = CO_2 + H$ (R34)	8.80×10^5	1.80	3.99×10^6
$CH_2O + H = HCO + H_2$ (R43)	4.10×10^8	1.50	1.02×10^7
$CH_2O + OH = HCO + H_2O$ (R46)	7.80×10^7	1.60	-4.41×10^6
$CH_2O + CH_3 = HCO + CH_4$ (R48)	3.20×10^1	3.40	1.80×10^7
$HCO = H + CO$ (R49)	9.90×10^{17}	−0.90	7.01×10^7
$HCO + H = CO + H_2$ (R50)	1.10×10^{14}	0	0
$HCO + OH = CO + H_2O$ (R53)	1.10×10^{14}	0	0
$CH3 + H + (M) = CH4 + (M^b)$ (R57)	2.10×10^8	0	0
low-pressure limit	6.47×10^{17}	−1.80	0
TROE centering	0.64, 1.00×10^{-28}	3.23×10^3	1.00×10^{30}
$CH_4 + OH = CH_3 + H_2O$ (R60)	1.00×10^6	2.20	1.05×10^7
$CH_3 + O = CH_2O + H$ (R67)	6.90×10^{13}	0	0
$CH_3 + OH = CH_2 + H_2O$ (R69)	1.10×10^3	3.00	1.16×10^7
$CH_3 + OH = CH_2(S) + H_2O$ (R70)	6.90×10^{14}	−0.50	0
$CH_3 + CH_3 + (M) = C_2H_6 + (M)$ (R78)	3.60×10^7	0	0
low-pressure limit	1.27×10^{35}	−7.00	1.15×10^7
TROE centering	0.62, 7.30×10^1	1.18×10^3	1.00×10^{30}
$CH_2 + H = CH + H_2$ (R81)	1.20×10^{14}	0	0
$CH_2 + CO_2 = CO + CH_2O$ (R91)	1.00×10^{11}	0	4.18×10^6
$CH_2(S) + (M) = CH_2 + (M^c)$ (R92)	1.10×10^{13}	0	0
$CH_2(S) + N_2 = CH_2 + N_2$ (R93)	1.30×10^{13}	0	0
$CH_2(S) + CO_2 = CH_2O + CO$ (R101)	1.10×10^{13}	0	0
$CH + H_2O = CH_2O + H$ (R107)	5.70×10^{12}	0	-3.16×10^6
$CH + CO_2 = HCO + CO$ (R108)	8.80×10^6	1.80	-4.35×10^6
$C + OH = CO + H$ (R109)	5.00×10^{13}	0	0
$CH_2OH + (M) = CH_2O + H + (M)$ (R122)	2.80×10^{14}	−0.70	1.37×10^8
low-pressure limit	6.01×10^{33}	−5.39	1.51×10^8
TROE centering	0.96, 6.76×10^1	1.86×10^3	7.54×10^3
$CH_2OH + H = CH_3 + H$ (R124)	1.80×10^{13}	0.20	4.64×10^5
$C_2H_4 + H = C_2H_3 + H_2$ (R199)	2.40×10^2	3.60	4.71×10^7
$CH_3 + CH_2 = C_2H_4 + H$ (R201)	1.20×10^{15}	−0.30	6.40×10^5
$C_2H_4 + OH = C_2H_3 + H_2O$ (R207)	1.30×10^{-1}	4.20	-3.60×10^6
$C_2H_2 + OH = HCCOH + H$ (R240)	2.40×10^6	2.00	5.32×10^7
$HCCO + H = CH_2(S) + CO$ (R330)	1.50×10^{14}	0	0

[a]Enhanced third-body efficiencies: H_2 = 2.5, H_2O = 12, CO = 1.9, and CO_2 = 3.8. [b]Enhanced third-body efficiencies: CH_4 = 1.9 and C_2H_6 = 4.8. [c]Enhanced third-body efficiencies: N_2 = 0, H_2O = 0, AR = 0, and H = 0.

These make the C_1 branch pathway more dominant under OCDR and OCWR. There are 29 elementary reactions that have a critical contribution to the modification of the production rate of intermediate species between AC, OCDR, and OCWR.

APPENDIX

Elementary reactions with great changes for their integrated oxidation rates under different combustion conditions (Table A1).

AUTHOR INFORMATION

Corresponding Author

*Telephone/Fax: +86-13971078291. E-mail: zliu@hust.edu.cn.

Notes

The authors declare no competing financial interest.

ACKNOWLEDGMENTS

This study is partially supported by the State Key Fundamental Research Project, Ministry of Science and Technology (MOST), under Grants 2011CB707301 and 2010CB227004, and the National Science Foundation of China (NSFC), under Grants 50936001 and 51021065. Lin Wang also thanks the help of Professor P. Glarborg and Assistant Professor Chang Bo Oh.

REFERENCES

(1) Wall, T.; Liu, Y. H.; Spero, C.; Elliott, L.; Khare, S.; Rathnam, R.; Zeenathal, F.; Moghtaden, B.; Buhre, B.; Sheng, C. D.; Gupta, R.; Yamada, Y.; Makino, K.; Yu, J. L. An overview on oxyfuel coal combustion—State of the art research and technology development. *Chem. Eng. Res. Des.* **2009**, *87*, 1003−1016.

(2) Buhre, B. J.; Elliott, L. K.; Sheng, C. D.; Gupta, R. P.; Wall, T. F. Oxy-fuel combustion technology for coal fired power generation. *Prog. Energy Combust. Sci.* **2005**, *31*, 283−307.

(3) Abián, M.; López, J. G.; Bilbao, R. Effect of different concentration levels of CO_2 and H_2O on the oxidation of CO: Experiments and modeling. *Proc. Combust. Inst.* **2011**, *33*, 317−323.

(4) Stadler, H.; Christ, D.; Habermehl, M.; Heil, P.; Kellermann, A.; Ohliger, A.; Toporov, D.; Kneer, R. Experimental investigation of NO_x emissions in oxycoal combustion. *Fuel* **2011**, *90*, 1604−1611.

(5) Tan, Y. W.; Croiset, E.; Douglas, M. A.; Thambimuthu, K. V. Combustion characteristic of coal in a mixture of oxygen and recycled flue gas. *Fuel* **2006**, *85*, 507−512.

(6) Weller, A. E.; Rising, B. W.; Boiarski, A. A.; Nordstrom, R. J.; Barrett, R. E.; Luce, R. G. *Experimental Evaluation of Firing Pulverized Coal in a CO_2/O_2 Atmosphere*; Argonne National Laboratory: Argonne, IL, 1985; ANL/CNSV-TM-168.

(7) Wang, C. S.; Berry, G. F.; Chang, K. C.; Wolsky, A. M. Combustion of pulverized coal using waste carbon dioxide and oxygen. *Combust. Flame* **1988**, *72* (3), 301−310.

(8) Abele, A. R.; Kindt, G. S.; Glark, W. D.; Payne, R.; Chen, S. L. *An Experimental Program to Test the Feasibility of Obtaining Normal Performance from Combustion Using Oxygen and Recycled Gas Instead of Air*; Argonne National Laboratory: Argonne, IL, 1987; ANL/CNSV-TM-204, DE89-002383.

(9) Yin, C.; Rosendahl, L. A.; Kær, S. K. Chemistry and radiation in oxy-fuel combustion: A computational fluid dynamics modeling study. *Fuel* **2011**, 2519−2529.

(10) Bhadraiah, K.; Raghavan, V. A numerical study of the effect of radial confinement on the characteristics of laminar co-flow methane−oxygen diffusion flames. *Proc. Inst. Mech. Eng., Part C* **2011**, *225*, 1213−1228.

(11) Park, J.; Hwang, D. J.; Choi, J. G.; Lee, K. M.; Keel, S. I.; Shim, S. H. Chemical effects of CO_2 addition to oxidizer and fuel streams on flame structure in H_2-O_2 counterflow diffusion flames. *Int. J. Energy Res.* **2003**, *27*, 1205−1220.

(12) Guo, H.; Galizzi, C.; Escudié, D. Effects of CO_2/N_2/Ar addition on liftoff of a laminar CH_4/air diffusion flame. *Proceeding of the Combustion Institute—Canadian Section Spring Technical Meeting*; Université de Montréal, Montreal, Quebec, Canada, May 11−13, 2009.

(13) Kim, G.; Kim, Y.; Joo, Y. J. Conditional moment closure for modeling combustion processes and structure of oxy-natural gas flame. *Energy Fuels* **2009**, *23*, 4370−4377.

(14) Andersen, J.; Jensen, P. A.; Meyer, K. E.; Hvid, S. L.; Glarborg, P. Experimental and numerical investigation of gas phase freeboard combustion. Part 1: Main combustion process. *Energy Fuels* **2009**, *23*, 5773−5782.

(15) Kim, H. S.; Shin, M. S.; Jang, D. S.; Lee, D. K. In-depth numerical analysis on the determination of amount of CO_2 recirculation in LNG/O_2/CO_2 combustion. *Appl. Therm. Eng.* **2010**, *30*, 616−622.

(16) Heil, P.; Toporov, D.; Förster, M.; Kneer, R. Experimental investigation on the effect of O_2 and CO_2 on buring rates during oxyfuel combustion of methane. *Proc. Combust. Inst.* **2011**, *33*, 3407−3413.

(17) Liu, F.; Guo, H.; Smallwood, G. J.; Gülder, Ö.L. The chemical effects of carbon dioxide as an additive in an ethylene flame: Implications for soot and NO_x formation. *Combust. Flame* **2001**, *125*, 778−787.

(18) Park, J.; Park, J. S.; Kim, H. P.; Kim, J. S.; Kim, S. C.; Choi, J. G.; Cho, H. C.; Cho, K. W.; Park, H. S. NO emission behavior in oxy-fuel combustion recirculated with carbon dioxide. *Energy Fuels* **2007**, *21*, 121−129.

(19) Smith, G. P.; Golden, D. M.; Frenklach, M.; Moriarty, N. W.; Eiteneer, B.; Goldenberg, M.; Bowman, C. T.; Hanson, R. K.; Song, S.; Gardiner, W. C.; Lissianski, V. V.; Qin, Z. W. http://www.me.berkeley.edu/gri-mech/version30/text30.html.

(20) Glarborg, P.; Alzueta, M. U.; Johansen, K. D. Kinetic modeling of hydrocarbon/nitric oxide interactions in a flow reactor. *Combust. Flame* **1998**, *115*, 1−27.

(21) Mendiara, T.; Glarborg, P. Ammonia chemistry in oxy-fuel combustion of methane. *Combust. Flame* **2009**, *156*, 1937−1949.

(22) Mendiara, T.; Glarborg, P. Reburn chemistry in oxy-fuel combustion of methane. *Energy Fuels* **2009**, *23*, 3565−3572.

(23) Glarborg, P.; Bentzen, L. L. B. Chemical effects of a high CO_2 concentration in oxy-fuel combustion of methane. *Energy Fuels* **2008**, *22*, 291−296.

(24) Kee, R.; Miller, J. A.; Evans, G. H.; Dixon-Lewis, G. A computational model of the structure and extinction of strained, opposed flow, premixed methane−air flames. *Proc. Combust. Inst.* **1988**, *22*, 1479−1494.

(25) Lutz, A. E.; Kee, R. J.; Grcar, J. F.; Rupley, F. M. *OPPDIF: A FORTRAN Program for Computing Opposed-Flow Diffusion Flames*; Sandia National Laboraories: Albuquerque, NM, 1997; Sandia Report SAND96-8243.

(26) Hwang, D. J.; Park, J.; Oh, C. B.; Lee, K. H.; Keel, S. I. Numerical study on NO formation in $CH_4-O_2-N_2$ diffusion flame diluted with CO_2. *Int. J. Energy Res.* **2005**, *29* (2), 107−120.

(27) Park, J.; Kim, K. T.; Park, J. S. A study on H_2−air counterflow flames in highly preheated air diluted with CO_2. *Energy Fuels* **2005**, *19*, 2254−2260.

(28) Nishioka, M.; Nakawaga, S.; Ishikawa, Y.; Takeno, T. NO emission characteristics of methane−air double flame. *Combust. Flame* **1994**, *98*, 127−138.

(29) Kee, R. J.; Rupley, F. M.; Miller, J. A. *CHEMKIN II: A Fortran Chemical Kinetics Package for the Analysis of Gas Phase Chemical Kinetics*; Sandia National Laboratories: Albuquerque, NM, 1989; Sandia Report SAND89-8009B.

(30) Kee, R. J.; Dixon-Lewis, G.; Warnatz, J.; Coltrin, M. E.; Miller, J. A. *A Fortran Computer Code Package for the Evaluation of Gas-Phase, Multicomponent Transport Properties*; Sandia National Laboratories: Albuquerque, NM, 1994; Sandia Report SAND86-8246.

(31) Grosshandler, W. L. *RADCAL: A Narrow-Band Model for Radiation Calculations in a Combustion Environment*; National Institute of Standards and Technology (NIST): Gaithersburg, MD, 1993; NIST Technical Note 1402.

(32) Barlow, R. S.; Smith, N. S. A.; Chen, J. Y.; Bilger, R. W. Nitric oxide formation in dilute hydrogen jet flames: Isolation of the effects of radiation and turbulence-chemistry submodels. *Combust. Flame* **1999**, *117*, 4−31.

(33) Frank, J. H.; Barlow, R. S.; Lundiquist, C. Radiation and nitric oxide formation in turbulent non-premixed jet flames. *Proc. Combust. Inst.* **2000**, *28*, 447−454.

(34) Zhu, X. L.; Gore, J. P.; Karpetis, A. N.; Barlow, R. S. The effect of self-absorption of radiation on an opposed flow partially premixed flame. *Combust. Flame* **2002**, *129*, 342−345.

(35) Barlow, R. S.; Karpetis, A. N.; Frank, J. H.; Chen, J. Y. Scalar profiles and NO formation in laminar opposed-flow partially-premixed methane/air flames. *Combust. Flame* **2001**, *127*, 2102−2118.

(36) Mostinsky, I. L.; Hewitt, G. F.; Shires, G. L.; Polezhaev, Y. V. *Diffusion Coefficient in International Encyclopedia of Heat and Mass Transfer*; CRC Press: Boca Raton, FL, 1996.

(37) Zhao, R.; Liu, H.; Zhong, X. J. Modeling of NO_x conversion during combustion under high CO_2 concentration using detailed chemical kinetics. *Fuel Process. Technol.* **2011**, *92*, 939−945.